Performance and Modeling of Antimonide-Based Heterostructure Backward Diodes for Millimeter-Wave Detection

P. Fay*, J. N. Schulman†, S. Thomas III†, D. H. Chow†,
Y. K. Boegeman†, and K. S. Holabird†

* Dept. of Electrical Engineering
University of Notre Dame, Notre Dame, IN 46556
tel: (574) 631-5693
fax: (574) 631-4393
email: pfay@nd.edu

† HRL Laboratories LLC, 3011 Malibu Canyon Rd.,
Malibu, CA 90265

Abstract

Heterostructure backward diodes have been fabricated and characterized for use as zero-bias millimeter-wave detectors. Sensitive detector performance in W-band was achieved by scaling the active area to 1.5x1.5 μm^2 through the use of high-resolution I-line stepper lithography. Responsivities of 2450 V/W and 2341 V/W were measured on-wafer at 95 GHz and 110 GHz, respectively. The detectors exhibit good detection linearity, with 0.8 dB compression measured at an RF power of 4 μW at 95 GHz. A nonlinear device model based on bias-dependent millimeter-wave s-parameter measurements has been developed. The model is consistent with the measured frequency response, responsivity, and detector compression characteristics. Extrapolation using the model to reduced device dimensions suggests that this device technology should provide appreciable responsivities (> 1000 V/W) at frequencies through G-band and beyond.

I. Introduction

Sensitive detectors at W-band and beyond have many potential uses, including applications in passive imaging arrays and radiometry. Of particular interest for arrays are zero-bias detectors since they obviate the need for bias control circuitry, simplifying the implementation of large arrays. Ge backward diodes [1] and planar-doped barrier diodes [2] can be used as zero-bias detectors at millimeter-wave frequencies, but have proven difficult to fabricate reproducibly in quantities sufficient for imaging array applications.

We report the millimeter-wave detection performance of InAs/AlSb/GaSb heterostructure backward diodes fabricated using high-resolution I-line stepper lithography for accurate definition of the small active areas needed for high sensitivity at W-band. The devices exhibit a strongly

0-7803-7478/02/$17.00 © 2002 IEEE

nonlinear current-voltage characteristic at zero applied bias, and have small associated capacitances as a consequence of the small device area facilitated by fine-line lithography. Measured device performance from dc-110 GHz and the development of a nonlinear device model that matches closely the experimental results are reported.

II. Device Design and Operation

The heterostructure used consists of an n-type InAs cathode (doped $7x10^{17}$ cm^{-3}), a 40 Å-thick AlSb barrier layer, and 200 Å of undoped $Al_{0.1}Ga_{0.9}Sb$, followed by a 500 Å p^+ GaSb anode (doped $4x10^{18}$ cm^{-3}) and an n^+ InAs anode contact layer. The staggered band alignment of GaSb to InAs facilitates this approach to low-resistance contacts to the anode side of the diode without the need for ohmic contact directly to the p-type GaSb.

The energy band diagram for this structure as calculated from a self-consistent Poisson/ Schrodinger solver [3] is shown in Figure 1. The doping level in the cathode contact layer was chosen in conjunction with the Al mole fraction in the AlGaSb barrier layer to place the Fermi level above the conduction band edge in the cathode and below the valence band edge in the AlGaSb simultaneously, as shown in Figure 1. As suggested by the band diagram in Figure 1, the staggered band alignment between AlGaSb and InAs facilitates a large reverse current due to interband tunneling. The forward current, on the other hand, is blocked by the bandgap of the AlGaSb layer. The resulting current-voltage characteristic exhibits strongly nonlinear behavior near zero bias, as desired for unbiased direct detection.

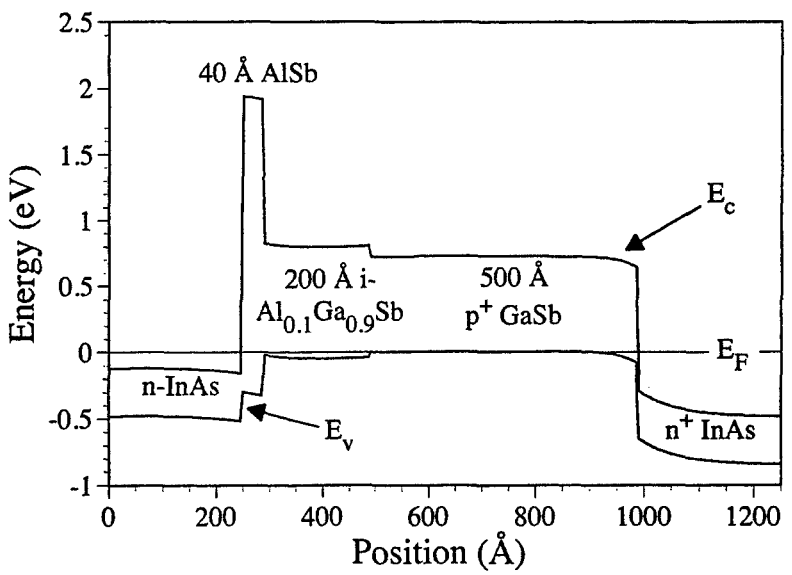

Figure 1. Calculated band diagram for Sb-based heterostructure backward diode detector.

Figure 2 shows the measured current-voltage characteristic of a typical 1.5x1.5 μm^2 area device. As can be seen, the IV curve is strongly nonlinear around zero applied voltage.

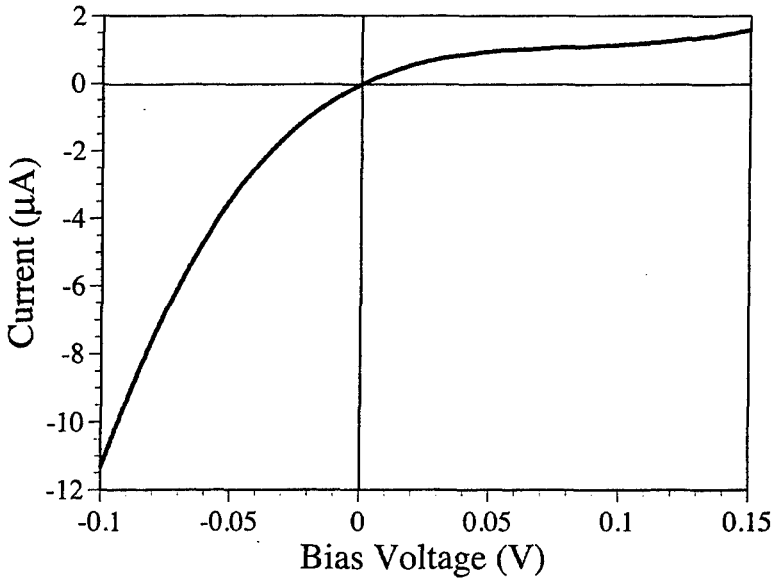

Figure 2. Measured current-voltage characteristic for a typical 1.5x1.5 μm² area device. Curvature at V=0 is 25.9 V⁻¹.

The curvature, $\gamma = \left(d^2I/dV^2\right)/\left(dI/dV\right)$, was measured to be 25.9 V-1 at V=0. The responsivity of the detector can be estimated from the curvature through the expression $\Re = 2Z_s\gamma$, where $\Re$ is the responsivity and Z_s is the RF source impedance [4]. This expression follows directly from the assumption of ideal square-law device behavior. For Z_s=50 Ω, this simple analysis suggests that the responsivity of these detectors should be approximately 2590 V/W. Higher-order nonlinearities and other effects not considered in this simple model are expected to cause the actual responsivity to deviate from this simple model.

III. Nonlinear Device Model

For the development of a nonlinear equivalent circuit model, on-wafer s-parameters were measured from 1-110 GHz as a function of externally applied bias. A network analyzer port power of -33 dBm was used to minimize distortion of the small-signal s-parameters due to device nonlinearity. The parameters for the equivalent circuit shown in Figure 3(a) were extracted as a function of applied bias. The bias dependence of junction capacitance, c_d, and conductance, g_d, are shown in Figure 3(b) for a typical 1.5x1.5 μm² area device. As can be seen in Figure 3(b), the conductance as extracted from the s-parameter measurements is nearly identical to the conductance determined from the derivative of the dc current-voltage characteristics. The absence of any detectable conductance dispersion suggests that no significant carrier trapping or surface effects are present in the device. The series resistance, r_s, was found to be approximately 14 Ω independent of applied bias.

A nonlinear device model based on these extracted parameters was implemented in a commercial harmonic balance simulator [5] using the equivalent circuit model in Figure 3. The

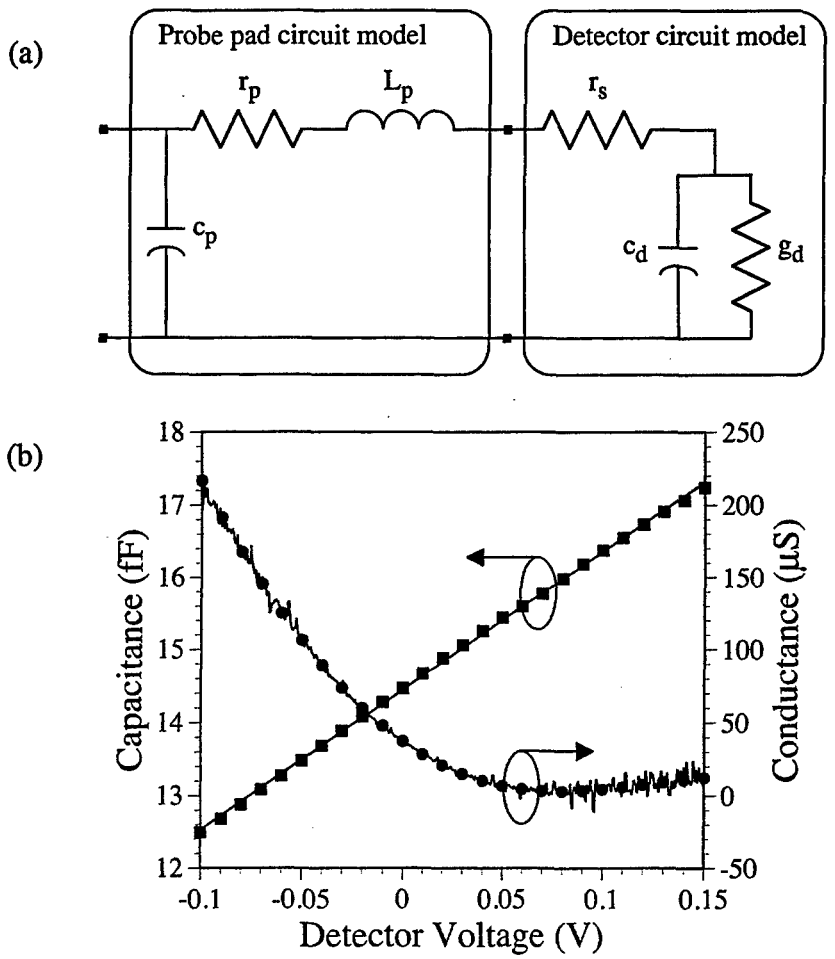

Figure 3. (a) Equivalent circuit for nonlinear circuit model. (b) Extracted junction capacitance (■) and conductance (●) from on-wafer s-parameter measurements from 1-110 GHz for a typical small-area device. Best-fit line through capacitance is shown, and conductance obtained from s-parameter measurements is superimposed over dc conductance for reference (solid line).

model is implemented as a nonlinear voltage-dependent current source for the junction conductance, and a voltage-dependent capacitor for the junction capacitance. The functional form of the current source was obtained by fitting a fourth-order polynomial to the extracted junction conductance vs. bias curve, and then integrating once with respect to voltage to obtain a current-voltage relation. The constant of integration was chosen to ensure that the dc current was zero at V=0. A least-squares linear fit to the extracted junction capacitance vs. applied voltage characteristic in Figure 3(b) was used to model the junction capacitance. Harmonic balance simulations using this model resulted in a predicted low-frequency detector responsivity of 2581 V/W. This is in good agreement with the value of 2590 V/W predicted from the ideal square-law model described previously. Examination of the relative contributions of various terms in the equivalent circuit model indicated that device series resistance is primarily responsible for the small observed deviation from the simple square-law model.

IV. High Frequency Detector Performance

The performance of the diodes as zero-bias detectors from 1 to 110 GHz was assessed through on-wafer measurements. The RF drive was supplied through a 1 mm coaxial cable and bias tee to a 100 μm pitch W-band Cascade wafer probe, and the detector voltage was measured using a microvoltmeter connected to the dc arm of the bias tee. Figure 4 shows the measured responsivity for a 1.5x1.5 μm^2 area detector as well as the result from simulations based on the nonlinear circuit model described above. For the measured data points shown, a source-impedance correction technique was used to remove the effects of the variation in wafer probe and millimeter-wave source impedance over the frequency range measured. The average measured responsivity over the frequency range from 1-50 GHz was 2597 V/W, consistent with the responsivity anticipated from the device model (2581 V/W). The frequency dependence of the responsivity predicted by the circuit model is also similar to that obtained by direct measurement, with both the measured and modeled responses starting to fall off for frequencies just above 100 GHz. At 110 GHz, the model predicts the responsivity should decline by 0.7 dB to 2390 V/W, while the measured responsivity at 110 GHz is 2341 V/W, 0.9 dB below the average responsivity from 1-50 GHz. The model predicts a -3 dB frequency for the responsivity of 187 GHz, which is beyond the maximum frequency attainable with the equipment currently available in the laboratory.

The maximum responsivity was also evaluated, as shown in Figure 4. For the modeled maximum responsivity curve shown in Figure 4, the source impedance was chosen to be conjugately matched to the detector equivalent circuit at the fundamental frequency. The low-frequency impedance-matched responsivity predicted by the model is $3.44x10^5$ V/W, and the responsivity at 95 GHz is $11.5x10^3$ V/W. For higher frequencies the responsivity falls to the

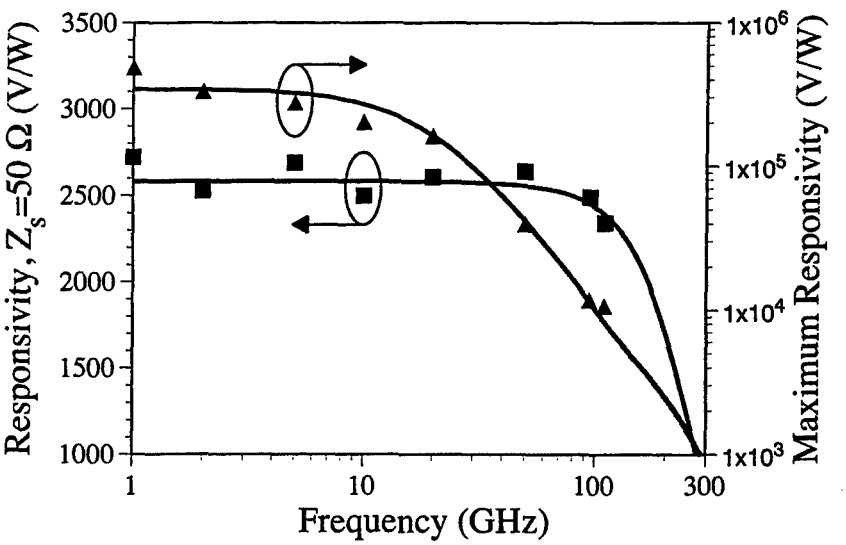

Figure 4. Measured and modeled responsivity vs. frequency for 1.5x1.5μm^2 area device. Data points (■) and curve referenced to left axis is for 50 Ω RF source; right axis data (▲) and curve is responsivity for conjugately-matched source impedance.

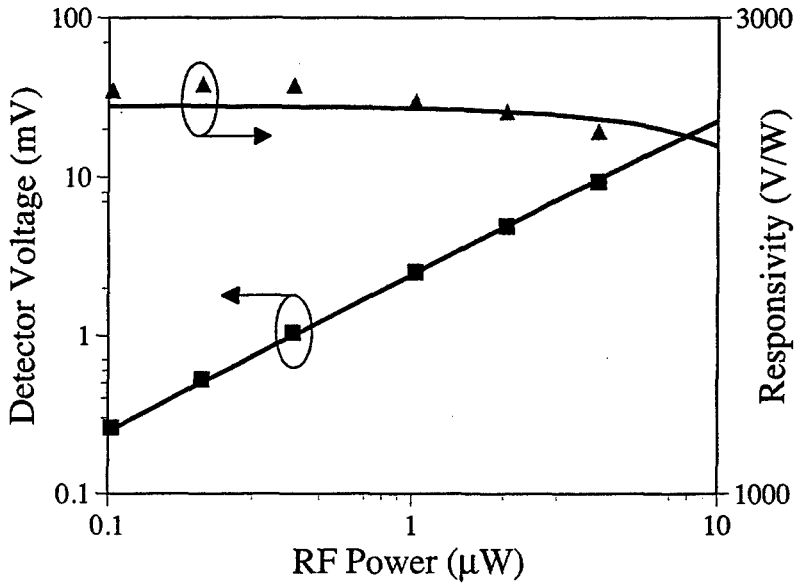

Figure 5. Measured and simulated detector voltage and responsivity vs. incident RF power at 95 GHz.

same magnitude as the low-frequency unmatched responsivity at 197 GHz, and to 1000 V/W at 286 GHz. As millimeter-wave tuners were not available to experimentally measure the impedance-matched responsivity directly, the unmatched measured responsivity data points, in conjunction with the measured s-parameters of the detectors, were used to project the responsivity that could be achieved with the inclusion of a lossless matching network between the source and detector. The measured Z_s=50 Ω responsivity, $\Re$, and measured S_{11} were used in the expression

$$\Re_{max} = \frac{\Re}{1-|S_{11}|^2}$$

to project the maximum responsivity experimentally; the results are plotted in Figure 4. Although this projection is approximate, neglecting in particular the effects of harmonic termination, it does give reasonably good agreement with the harmonic balance simulation.

The dependence of responsivity on incident RF power was also measured on-wafer as well as assessed through simulations using the device model. Figure 5 shows the measured and modeled responsivity vs. incident RF power at 95 GHz for a typical 1.5x1.5 μm^2 area detector. The measured and modeled detector dc voltage and responsivity track each other closely over almost the entire range of experimentally-accessible power levels. The maximum power in the experiments was limited to approximately 4 μW by the millimeter-wave source and cable losses. Compression of the responsivity by approximately 0.8 dB is observed experimentally for an incident power of 4 μW. The equivalent circuit model is somewhat optimistic in this regard, predicting a smaller drop in responsivity (0.3 dB) at 4 μW. At a drive level of 4 μW, the peak-to-peak voltage impressed across the diode due to the RF drive is approximately 80 mV due to the high diode impedance. This voltage swing is approaching the limits of validity of the

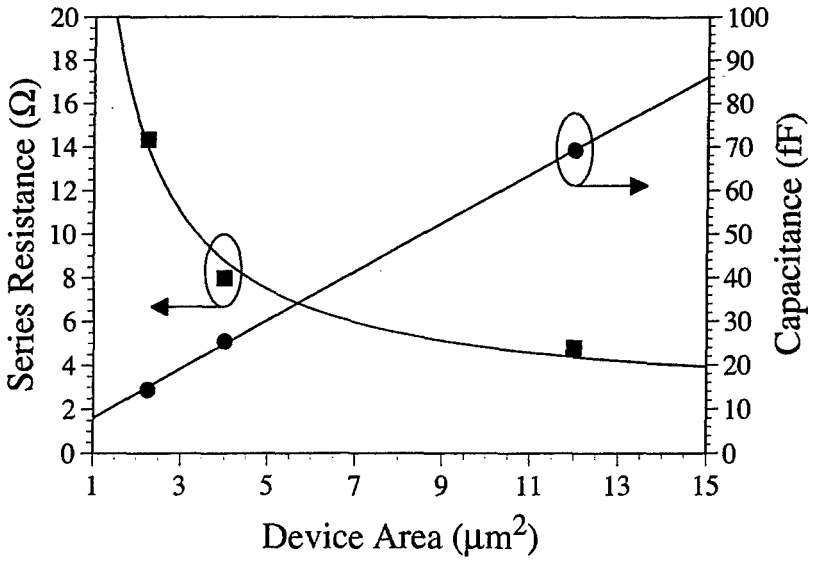

Figure 6. Scaling trends for series resistance(■) and device capacitance (●) obtained from fitting parameters of equivalent circuit to measured s-parameters of devices with varying areas.

current circuit model. Characterization of the devices over a larger bias range and use of higher-order fitting functions may be required to achieve better agreement at high drive levels.

V. Device Scaling and Optimization

The dependence of detector performance on diode area was investigated by characterizing devices with active areas ranging from 3x4 μm^2 to 1.5x1.5 μm^2. On-wafer s-parameter measurements of devices of different areas were made, and the circuit model shown in Figure 3 was extracted for devices of each size. The scaling trends for series resistance and junction capacitance are shown in Figure 6. Least-squares fitting to the extracted series resistance and junction capacitance resulted in the scaling relations

$$r_s = 26.65\ \Omega\mu m^2/A + 2.15\ \Omega$$

$$c_d = 5.58\ fF/\mu m^2 A + 2.49\ fF$$

where A is the device area. The series resistance very nearly follows the expected inverse-area scaling, with the addition of a small offset resistance. Similarly, the diode capacitance was found to be nearly proportional to area except for a small additional parasitic component.

The scaling trends in series resistance and diode capacitance give rise to an optimal device area that maximizes detector bandwidth. For devices based on this heterostructure and fabrication process driven from a millimeter-wave source with Z_S=50 Ω, this optimum device area is approximately 0.19 μm^2. The I-line stepper used to fabricate the devices reported here has previously demonstrated the ability to print 0.4x0.4 μm^2 features, suggesting the feasibility of such a scaled device in this fabrication technology. Figure 7 shows the projected responsivity for a 50 Ω source and a conjugately-matched source vs. frequency for such an optimally-sized

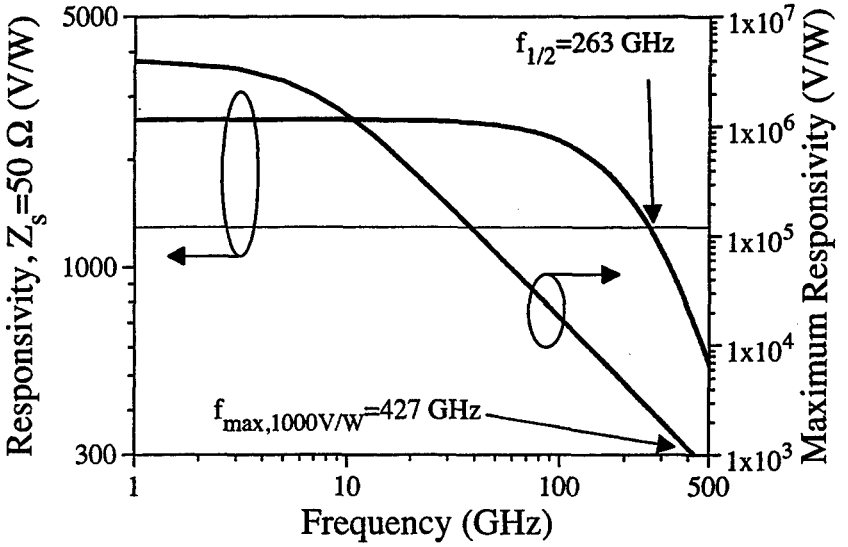

Figure 7. Projected responsivity vs. frequency for an optimally scaled 0.19 μm² area device. Responsivity with Z_s=50 Ω is 1/2 its low-frequency value at 263 GHz, while the conjugately-matched responsivity is > 1000 V/W for frequencies up to 427 GHz.

detector, as determined from the harmonic balance model using the scaling relations shown above. The Z_S=50 Ω responsivity drops to 1/2 of its low-frequency value at 263 GHz, while an impedance-matched detector exhibits a responsivity greater than 1000 V/W up to 427 GHz. Within the limitations of the circuit model, these Sb-based heterostructure backward diodes appear to be promising candidates for applications through G-band and beyond.

VI. Conclusions

The performance of antimonide-based heterostructure backward diodes as sensitive zero-bias detectors at millimeter-wave frequencies has been investigated. An average responsivity of 2597 V/W has been obtained experimentally from 1-50 GHz, and millimeter-wave responsivities of 2450 V/W and 2341 V/W at 95 GHz and 110 GHz, respectively, have been obtained. A nonlinear equivalent circuit model based on bias-dependent small-signal s-parameter measurements that is suitable for use with commercial harmonic balance simulators has been developed. The model has been verified using on-wafer responsivity and responsivity compression measurements of devices, and found to closely mirror the experimental data. The model has been used to predict the performance of a scaled detector, and suggests that this device technology should be suitable for detection at G-band and above.

VII. Acknowledgements

The authors wish to thank A. Seabaugh for the use of his 8510XF network analyzer for s-parameter measurements, M. Morgan and S. Weinreb for sharing their preliminary analyses of similar heterojunction detectors, and L. Warren and H. Dunlap for technical assistance.

VIII. References

[1] C. A. Burrus Jr., "Backward diodes for low-level millimeter-wave detection," *IEEE Trans. Microwave Theory and Techniques*, vol. 11, pp. 357-362, 1963.

[2] M. J. Kearney, A. Condie and I. Dale, "GaAs planar doped barrier diodes for millimetre-wave detector applications," *Electronics Lett.*, vol. 27, pp. 721-722, 1991.

[3] I. H. Tan, G. L. Snider, and E. L. Hu, "A Self-Consistent Solution of Schrodinger-Poisson Equations Using a Nonuniform Mesh," J. of Applied Physics, Vol. 68, pp. 4071-4076, 1990.

[4] J. N. Schulman, E. T. Croke, D. H. Chow, H. L. Dunlap, K. S. Holabird, M. A. Morgan, and S. Weinreb, "Quantum Tunneling Sb-Heterostructure Millimeter-Wave Diodes," *IEDM Tech. Digest*, pp. 765-767, 2001.

[5] Advanced Design System, version 1.90. Agilent Technologies, Palo Alto, CA 94304.